Robust Fitting of Geometric Primitives on LiDAR Data

Tekla Tóth and Levente Hajder
Department of Algorithm and Applications, Eötvös Loránd University,
Pazmany Peter stny. 1/C, Budapest 1117, Hungary

Keywords: Surface Fitting, Geometric Primitives, Light Detection and Ranging, Robust Fitting.

Abstract: This paper deals with robust surface fitting on spatial points measured by a LiDAR device. The point clouds contain hundreds of thousands data points. Therefore, the time demand of the algorithms is crucial for fast operation. We present two novel algorithms based on the RANSAC method: one for plane detection and one for other object detection. The execution time of the novel algorithms is significantly lower as only one random sampling is required because a deterministic teqnique selects the other data points. The accuracy of the novel methods are validated on synthesized data as well as real indoor and outdoor measurements.

1 INTRODUCTION

3D vision (Hartley and Zisserman, 2003) is one of the most challenging research topic of computer science. There are many different sensors for machine perception systems that can produce accurate spatial data from our 3D world. Vision applications are usually based on digital cameras. However, other sensors become popular recently.

The aim of this paper is to show that LiDAR (Light Detection And Ranging) technology can be effectively used for 3D object detection. It is a surveying method that measures distance to a target by illuminating the target with pulsed laser light and measuring the reflected pulses with a sensor. Differences in laser return times and wavelengths can then be used to create digital 3-D representations of the target. (Definition of LiDAR is from Wikipedia (TM)).

It is demonstrated in this paper that the accuracy of a LiDAR scans is enough to detect geometric primitives such as planes, spheres and cylinders. The former and the latter ones are especially important objects as they usually appear in real-world scenes: the ground and the walls of the buildings are planes, and advertising columns and lamp posts form cylinders.

The challenge of 3D object fitting algorithms is that LiDAR devices can scan only one side of the object, because more than half of the objects are occluded.

1.1 Related Work

Fitting geometric primitives on LiDAR point clouds is a relatively new research topic. The main idea here is to adapt efficient fitting methods to point clouds taken by LiDAR devices.

This paper deals with the fitting of planes, spheres and cylinders. The latter two tasks are more challenging as only part of the object can be measured due to self-occlusion. Plane fitting seems to be significantly simpler, but this task can be speeded up if specialties of urban scenes are considered.

Plane Fitting. LiDAR technology has become popular for the last decade although the price of the devices are quite high. To the best of our knowledge, the first solved task using LiDAR was the plane fitting (Tsai et al., 2010) which is a long-time researched problem in 3D geometry with efficient solutions (Pratt, 1987; Eberly, c; Eberly, b). Detected planes can be used for several purposes, e.g. motion registration (Grant et al., 2013) or reconstruction of buildings via roof detection (Awrangjeb and Fraser, 2014).

Sphere Fitting. Although spheres are relatively simple geometric objects that can be reconstructed efficiently (Eberly, c), the detection of spheres on LiDAR data is not frequently addressed, maybe because spheres do not usually appear in urban environment. However, (Pereira et al., 2016) showed that spheres are very useful for registering different point clouds, taken by LiDAR devices, into a common system.

Tóth, T. and Hajder, L.
Robust Fitting of Geometric Primitives on LiDAR Data.
DOI: 10.5220/0007572606220629
In *Proceedings of the 14th International Joint Conference on Computer Vision, Imaging and Computer Graphics Theory and Applications (VISIGRAPP 2019)*, pages 622-629
ISBN: 978-989-758-354-4

Cylinder Fitting. Cylinder fitting (Eberly, a) is more challenging than reconstruction of spheres, nevertheless, advertising columns often appear in large cities, therefore cylinder fitting is a realistic problem for machine perception. To the best of our knowledge, cylinder fitting is addressed only on laser scanned data (Nurunnabi and andoderik Lindenbergh, 2017).

In this paper, we show how planes, spheres, and cylinders can be reconstructed from LiDAR point clouds. The main challenge of these problems is that only part of the observed object is visible due to self-occlusion. The contributions of our paper are as follows: (i) a novel modification of RANSAC algorithm is introduced for robust plane fitting; another similar modification is applied for sphere and cylinder fitting. (ii) The appendix contains basic and precise geometric methods for plane, sphere and cylinder fitting that can yield accurate object parameters even if the methods are supported by LiDAR data; (iii) The efficiency of the methods are validated both on synthesized and real data-world data.

2 PROPOSED METHODS

In this section, we introduce novel robust fitting methods. Development issues are also discussed here.

2.1 Robust Model Estimation

Our shape detection is based on RANSAC (Fischler and Bolles, 1981) (RAndom SAmpling Consensus) algorithm. RANSAC is a method which fits a model from randomly sampled subset of an observed dataset. It works with arbitrary model. For line fitting, the basic steps of the RANSAC algorithm is visualized in Figure 1. These are as follows:

1. Randomly select a subset from the original dataset. Usually, the size of the subset is the minimal one. For example, two/three points are selected for line/plane fitting.
2. Model is fitted to the selected subset.
3. Classification of all the points of the dataset to inliers/outliers based on an error function. For line/fitting, a point is an inlier if it is closer to the line/plane than a given threshold. It is a disadvantage of the method that this threshold is usually given empirically. The set of inliers is called consensus set..
4. The estimated model is accepted if the consensus set is large enough.
5. Modification of the accepted model by refitting it from the inliers.

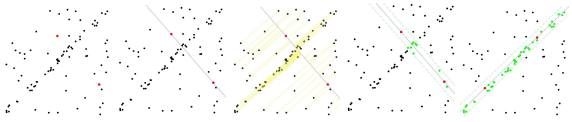

(a) Step 1 (b) Step 2 (c) Step 3 (d) Step 4-5 (e) Step 6

Figure 1: Illustration of RANSAC algorithm for line fitting. The titles of the subfigures denote the steps of the algorithm.

6. Repeat steps 1-5 several times. Repetition number can be calculated if outlier ratio is approximately known. If we reach one or more successfully fitted results, the model with the largest consensus set is chosen.

RANSAC is a reliable method. However, for multi-model fitting it is not a viable solution as the number of iterations is extremely high if only a small portion of the data points belong to an object. Table 1 shows the required number of iterations. Remark that at least three data points are necessary for plane and cylinder fitting, while spheres require more than that.

If only five percent of the dataset corresponds to a plane, more than 36.000 iterations are required to obtain good result with 99% probability. It is very time-consuming even if GPU is applied for the computation.

2.1.1 Plane Detection

The original algorithm can be parallelized to make it faster, but there are several properties in case of LiDAR point clouds which can improve the algorithm. Our modified RANSAC algorithm of plane detection is based on two observations.

Observation 1. The planes in urban environment are principally the ground or the walls of the buildings, hence they contain a huge amount of points, up to half of the whole cloud. Therefore, one can reduce the search time with sampling, and we can construct a more focused detection algorithm.

Table 1: Number of iterations required for original RANSAC (Fischler and Bolles, 1981) algorithm if confidence is set to 99%. N denotes the number of sample points. Both plane and cylinder fitting requires at least 3 points. For sphere fitting, the minimum number is 4. Columns are varying w.r.t. outlier ratio from 50% to 95%. It is well seen that $N = 1$ case is drastically faster than the others.

N	50%	65%	80%	90%	95%
1	7	11	20	44	90
3	35	106	573	4602	$\sim 10^4$
4	72	305	2875	$\sim 10^4$	$\sim 10^5$

Observation 2. The normal vectors of the planes are usually either vertical or horizontal. With minimal

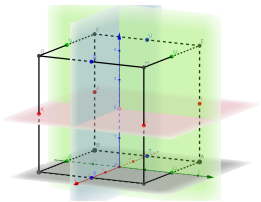

Figure 2: Synthetic point generation and the planes along the synthetic directions, yielding sets Ω_x (green), Ω_y (blue), Ω_z (red).

rotation can be reached that the planes are parallel to two of the three coordinate axes.

Instead of taking a subset of sampling points, we choose only one point $\mathbf{P} = (p_x, p_y, p_z)$ of the original set. Four synthetic points are calculated along the three planes perpendicular to the axes of the coordinate system with a given t distance in the following way, yielding point sets Ω_x, Ω_x, and Ω_z as

$$\begin{aligned}\Omega_x = \{&(p_x, p_y, p_z), (p_x, p_y + t, p_z + t), (p_x, p_y + t, p_z - t),\\ &(p_x, p_y - t, p_z + t), (p_x, p_y - t, p_z - t)\}\\ \Omega_y = \{&(p_x, p_y, p_z), (p_x + t, p_y, p_z + t), (p_x + t, p_y, p_z - t),\\ &(p_x - t, p_y, p_z + t), (p_x - t, p_y, p_z - t)\}\\ \Omega_z = \{&(p_x, p_y, p_z), (p_x + t, p_y + t, p_z), (p_x + t, p_y - t, p_z),\\ &(p_x - t, p_y - t, p_z), (p_x - t, p_y - t, p_z)\}.\end{aligned} \tag{1}$$

This calculation is illustrated in Figure 2. Assume that the red, green and blue colors denote axes X, Y and Z. In the figure, the coordinates of point $\mathbf{P}$ is $(0,0,2)$, and the distance threshold parameter is set to $t = 2$. The synthetic points of Ω_x, Ω_y and Ω_z are the middle point of the edges: there are four green, four blue and four red points.

The input points of the plane fitting algorithm are the closest real points in the pointcloud to the synthetic points. Point $\mathbf{P}$ is unchanged, but the other four points are replaced for the closest one in the whole pointcloud. We evaluate the minimal needed distance from $\mathbf{P}$ during the tests. Furthermore, if the plane searching parameter is t, the algorithm can detect the planes, rectangles with area least t^2.

After searching the closest real points, one can fit the planes to Ω_x, Ω_y and Ω_z sets. Thus the three principal planes, drawn by red, blue, and green in the figure, are separately processed, they obtain three different candidate planes. Then the consensus set of all the planes is collected similarly to the original RANSAC algorithm.

2.1.2 Sphere and Cylinder Detection

In case of a sphere or a cylinder, we can use a similarly modified RANSAC algorithm. However, the result depends on more parameters. After plane detection, the remaining surfaces are built from partly

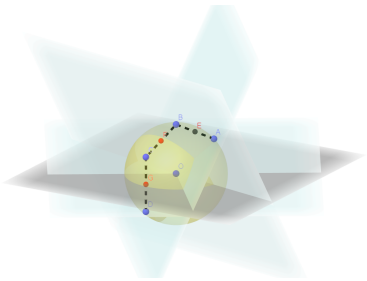

Figure 3: Estimation of the sphere center. Each candidate point pair of the sphere determines a plane. The sphere center is the intersections of these planes.

covered but continuous pointsets and they are easily separable in space. Hence the search to find the candidate spherical and cylindrical objects can run in parallel. The algorithm randomly chooses a single point and takes the closest points within a predefined distance. The inliers are the points with neighboring point which Euclidean distance is smaller than a given threshold parameter t. When the pointset contains less then k points, it is discarded. k are set in an empirical way, see the test section for our setting. Then the surface fitting is carried out on the selected points, yielding a candidate model. The further steps are similar to the original RANSAC. The final model contains the most inliers.

2.2 Surface Fitting Methods

The main goal is to detect planes, spheres and cylinders from noise point clouds, therefore very effective and robust fitting algorithms are needed. We suggest efficient fitting methods, the suggested algorithms are written in the Appendix in detail. However, in case of the LiDAR data, we have to modify the algorithms, because of the special properties of the LiDAR point clouds. The following two subsection introduce our new methods for sphere and cylinder fitting.

Estimation of the Center of a Sphere. A good estimation for the center of the sphere is the average of the sample points, as it is discussed in the appendix if the surface of the sphere is uniformly sampled. However, this is a bad approximation in case of LiDAR data where only one segment of the sphere is known, because this solution needs too many iterations.

We implemented our method based on a geometrical approach, which is visualized in Figure 3. The center of the sphere can be estimated from the equations of its four points. Bisecting plane of two points contains the center itself, and the intersection of three bisecting planes is a good estimation for the center.

To our experience, 10 points are enough to select because synthetic tests showed that it is an accurate

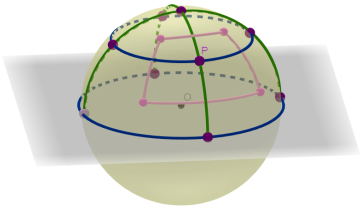

Figure 4: Hemisphere of the possible directions of the cylinder. The initial step evaluates the errors at the purple points. Pink points denote the directions after bisecting the initial intervals.

estimation, and more points yield increased computation time. Hence when there is a larger input pointset, one can get a good estimation using 10 randomly chosen points. After this, the fixpoint-iteration gives the local optimal solution.

Estimation of the Direction of the Cylinder. To estimate the direction of the cylinder axis, we represent vector **W** with a two dimensional parameter. Vector **W** with spherical coordinates is given by Equation 4. The original method, written in the appendix, finds this vector by exhaustive search. It splits the interval of the two parameters into 1024 and 512 equal parts. This gives a very accurate result because of the fine sampling.

However, most of the calculations are unnecessary. To reach the same result, an incremental approximation is applied, yielding significantly less time demand. Figure 4 shows the initial step of the method, where the hemisphere represents the set of the possible unit length directional vectors. At first, we calculate the fitting error in the nine directions denoted by the purple points, which are obtained by the equal partitioning of the intervals of θ_0 and θ_1 into 4 and 3 parts, respectively. If the direction of minimal error value is the labeled by point **P**, the optimal direction is located within the pink part of the sphere. Thereafter we iteratively bisect the intervals of θ_0 and θ_1 until the desired accuracy is reached.

3 TESTS AND RESULTS

The proposed algorithms are implemented in MATLAB. The methods are tested both on synthetic and real LiDAR datasets. The synthetic tests and indoor data, measured by Velodyne HDL-64 and Velodyne VLP-16-LiDAR, are made for sphere and cylinder fitting, and the outdoor data is designed to fit planes and cylinders.

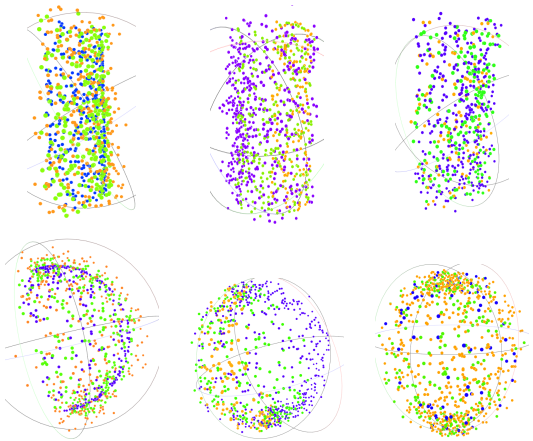

Figure 5: Synthetic datapoints for cylinder (up) and sphere fitting (down). Left: Noise added to points. Middle: Occluded points removed. Right: pointset made sparser. In the figures, blue dots represent original pointset, green when the noise/point removing is moderate, yellow when high amount of noise/point removing is applied. *Best viewed in color.*

3.1 Test Data

The synthetic tests contain randomly generated points of a plane, sphere or cylinder with given parameters. The results were observed in the presence of growing noise, occlusion and the number of the sample points.

The real tests are indoor and outdoor LiDAR measurements. The difficulty is, that the HDL-64 data is very noisy, and the outdoor data is only available with this device, which was equipped on a car. The indoor tests were made in a room with exact test objects, however, the scene were fully continuous against the street tests.

3.2 Synthetic Tests

In order to quantitatively test the robust fitting methods, synthetic test sequences are generated. The main goal for the test generation is to simulate the real measurement. For this reason, three parameters can be changed in our environment:

1. **Noise.** LiDAR technology has been improved for the last decade, yielding more accurate measurements. The precision of Velodyne HDL-64 is approximately 100 mm, that of VLP-16 is a bit smaller. Remark that Velodyne VLP-16 is the newer technology.
2. **Occlusion.** Normally, 3D scanning by a LiDAR device can measure only one side of an object due to self-occlusion. This effect can also be simulated in our testing environment.

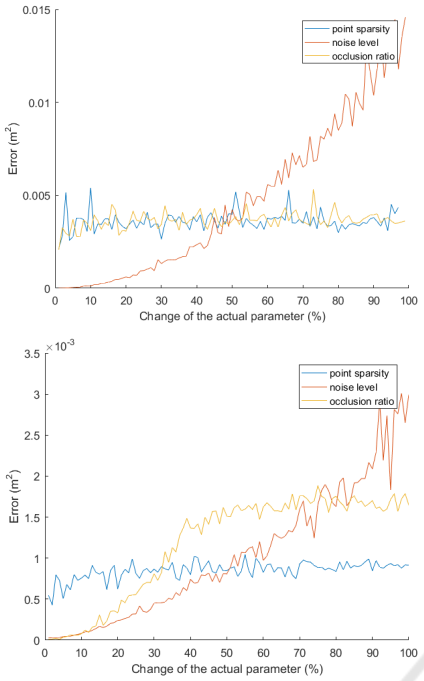

Figure 6: Error of sphere (top) and cylinder (bottom) fitting. Data are synthetically generated. Red, yellow, and blue curves are noise level, occlusion ratio, and point sparsity, respectively. Vertical axis shows the fitting error. Best viewed in color.

3. **Density of the Point Cloud.** For real measurement, density is determined by the applied LiDAR device. It mainly depends on the number of the beams. E.g. Velodyne HDL-64 and VLP-16 have 64, and 16 beams, the point cloud measured by the former one is significantly denser.

For the synthesized tests, a sphere with 0.375 m radius, and a cylinder with 1.3 m height and 0.35 m radius are generated. The fitting of the two objects are separately tested. The objects are translated in order to make them viewable from the location of the synthesized LiDAR. The object is rotated as well, however, it does not influence the sphere fitting as spheres are rotational symmetric.

Then noise is added to all the points in order to simulate the measurement noise of the LiDAR technique. Finally, points are removed to simulate self-occlusion and measurement by sparse devices. The synthesized spheres and cylinders are visualized in Figure 5.

Test results are plotted in Figure 6. The three different test types are visualized in the same chart. They are distinguished by different colors.

The tests show that the fitting quality is principally based on noise in both cases as the error increases monotonically. The influence of the self-occlusion is not significant, but the sparsity of the point cloud affects the results of the cylinder. These tests are run 100 times because of the random parameters, and the same results are obtained.

As it is expected, the error is increasing in all test cases: it is evident that noise, self-occlusion and point removal make a fitting less accurate.

3.3 Real Indoor Tests

The fitting methods are tested on point clouds taken in both indoor and outdoor environment. The indoor tests are discussed first. Some examples for sphere and cylinder fitting are shown in Figure 7 and 8.

An important task of the experiments is to tune the free parameters of the algorithms on real datasets. In case of plane detection, it is observed that if the distance between the real point and the one generated by the proposed method is less or equal than 5 cm, the result becomes inaccurate. Furthermore, the optimal value of t is between 0.3 and 0.5 m, hence the algorithm detects planes with dimensions greater than $[0.6 \times 0.6] - [1.0 \times 1.0]$m. The plane detector requires some trade-offs near the line where two planes cut each oder. The first time detected plane contains all points inside the threshold t from both planes. So if t is higher, the fitting is very inaccurate, but if t is lower, many good points are lost. For practical reasons, we implemented a re-selection of the points near these cutting lines.

The improved RANSAC needs less iterations, because it has to select only a single point from a plane, the other four points are generated synthetically. If we run the algorithms with the same iteration number, the modified algorithm selects the greatest plane more times, so we get more accurate result.

The parameter t is set to 0.4 m in case of sphere and cylinder fitting, because real tests contains cylinders with $1-2$ m height. The minimal number of points (k) is 15, because it approaches the expected fitting. Moreover, the improved sphere fitting algorithm needs one fifth of the iterations to reach the same sphere parameters as the original method.

3.4 Real Outdoor Tests

Outdoor tests are taken to test the plane and cylinder fitting algorithm. There are many planes in urban environment: the ground, building walls, side of vehicles, etc. Cylinders also appear near the roads: advertising columns can be modeled as regular cylinders. Unfortunately, sphere testing is missing in the case of outdoor testing as regular spheres do not appear in cities to the best of our knowledge.

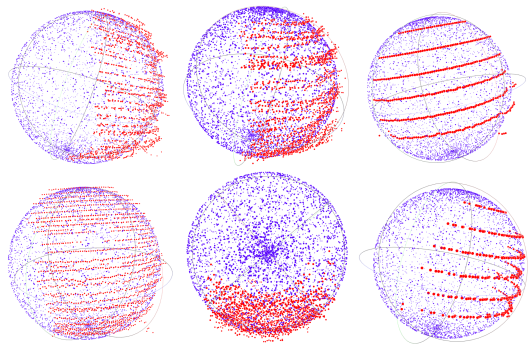

Figure 7: Fitted spheres. Point clouds in the left two columns were taken by Velodyne HDL-64, right columns by VLP-16. Red and blue dots visualize the measured and fitted data, respectively. The self-occlusion is the highest in the middle column.

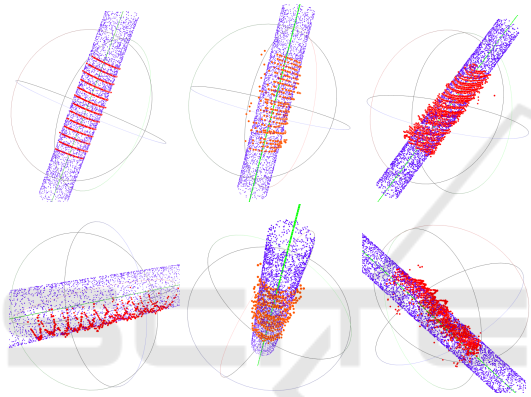

Figure 8: Fitted cylinders. Point clouds in the right two columns were taken by Velodyne HDL-64, left columns by 16. Red and blue dots visualize the measured and fitted data, respectively. The self-occlusion is the highest in the middle.

Figure 9 shows an example for plane fitting. The point cloud is taken in a crossroads where five vertical walls around the measuring device. All of them are successfully segmented. They are plotted by different colors in the figure. Table 2 consists of the time demand, in seconds, of the original RANSAC and our modified algorithm on this test scenario.

There are challenges even for plane fitting: disadvantage of noisy points is demonstrated in Figure 10, where the points of the same plane form different quasi-parallel planes because of the mirroring of the widows. It seems to impossible to filter out these planes, because they really create false planes in the pointcloud. The obtained plane parameters of this example are shown in Table 3.

Geometrically, advertising columns or lamp posts are cylinders. However, the number of the points corresponding to this objects are not too high. Real examples for cylinder fitting is visualized in Figure 11, the obtained parameters are listed in Table 4.

Table 2: Time demand of the plane detectors. $T_{original}$ and $T_{proposed}$ denote the original RANSAC and the proposed algorithm. Test results are visualized in Figure 9. Tests were run 1000-times and average values are listed.

	color	N	$T_{original}$	$T_{proposed}$
1.	green	52857	**16.434**	17.945
2.	yellow	4904	10.323	**9.675**
3.	red	2239	8.932	**7.830**
4.	light blue	2101	7.525	**7.333**
5.	dark blue	1866	7.292	**6.752**
6.	magenta	1518	7.043	**6.425**
7.	orange	1344	6.992	**6.182**

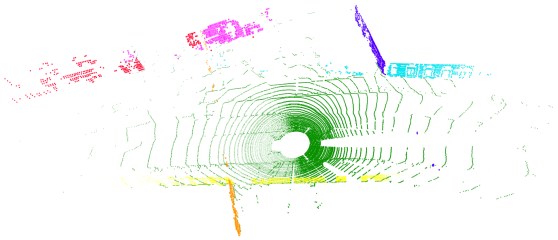

(a) Outdoor measurement

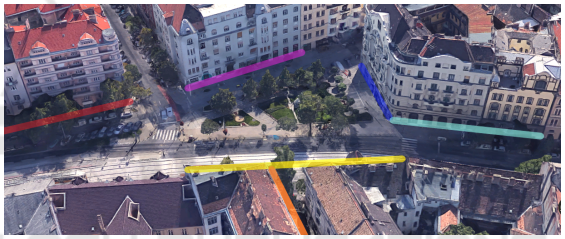

(b) Real environment

Figure 9: The figure shows the similarity between the fitted planes to an outdoor measurement, and the map of the real environment. *Best viewed in color.*

4 CONCLUSION

The paper proposes novel fitting algorithms which can reconstruct sphere, cylinder and plane. The goal was to detect and reconstruct the given objects in a sparse pointcloud.

The fitting algorithms are efficient and fast. The RANSAC algorithm is modified to get fewer iteration, decreasing the time demand. This modification is based on some special properties of the sparse point cloud taken of urban environments.

The methods are tested on synthetic point clouds, varying the amount of noise, the number of the points and the self-occlusion. Real indoor and outdoor test results are also presented, the advantages and limits of the algorithms are discussed.

Table 3: Parameters of the detected planes in Figure 10. N denotes the number of points for which the plane fitting is carried out. Vectors $\mathbf{P_0}$ and $\mathbf{n}$ denote a point of the plane, and the plane normal. Five out of the six plane are quasi parallel, the blue one is perpendicular to the others.

	color	N	$\mathbf{P_0}$	$\mathbf{n}$
1.	green	31 743	(1.881, 0.999, -0.191)	(-0.098, -0.995, 0,013)
2.	magenta	10 328	(-2.486, 0.998, -1.071)	(-0.059, -0.959, 0.055)
3.	purple	9007	(-1.394, 0.996, 0.7974)	(-0.235, -0.961, -0.148)
4.	rose	4076	(-2.203, 0.989, -1.2377)	(0.021, -0.940, 0.340)
5.	blue	5698	(0.459, -0.041, 5.0901)	(0.893, -0.449, 0.013)
6.	orange	2428	(-2.086, 0.976, -0.572)	(-0.143, 0.867, 0.478)

Table 4: Parameters of the detected cylinders in Figure 11. N denotes the number of the points of a cylinder. Vectors $\mathbf{C}$ and $\mathbf{W}$ denote a point of the axis and the direction of the axis. r and h are the radius and the height value of the cylinder, finally, E denotes the fitting error given in Euclidean distance.

	N	$\mathbf{C}$	$\mathbf{W}$	r	h	E
1.	660	(5.560, 0.029, -0.432)	(0.000,0.000, 1.000)	0.127	2.257	0.001
2.	782	(6.203, 7.609, -0.174)	(-0.024,0.074, 0.996)	0.559	2.464	0.002
3.	263	(6.687, 16.955, 0.340)	(0.000,0.078, 0.996)	0.487	2.352	0.006

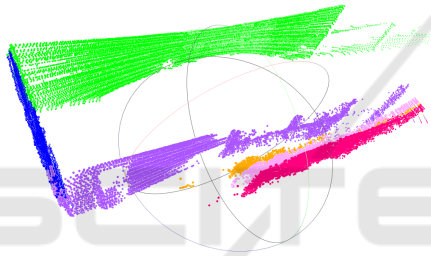

Figure 10: Fitted planes of an outdoor test in case of high noise because of mirroring.

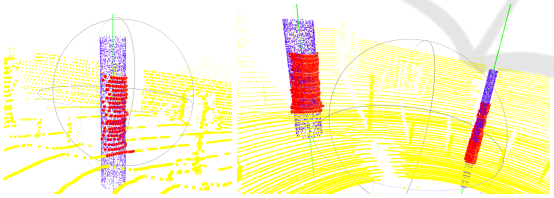

Figure 11: Fitted cylinders of some outdoor measurements.

ACKNOWLEDGEMENTS

EFOP-3.6.3-VEKOP-16-2017-00001: Talent Management in Autonomous Vehicle Control Technologies – The Project is supported by the Hungarian Government and co-financed by the European Social Fund.

REFERENCES

Awrangjeb, M. and Fraser, C. S. (2014). Automatic segmentation of raw LIDAR data for extraction of building roofs. *Remote Sensing*, 6(5):3716–3751.

Björck, Å. (1996). *Numerical Methods for Least Squares Problems*. Siam.

Eberly, D. Fitting 3D Data with a Cylinder. http://www.geometrictools.com/Documentation/CylinderFitting.pdf. Online; accessed at 5th November 2018.

Eberly, D. Least Squares Fitting of Segments by Line or Plane. https://www.geometrictools.com/Documentation/FitSegmentsByLineOrPlane.pdf. Online; accessed at 5th November 2018.

Eberly, D. Least Squares Fitting on Data. http://www.geometrictools.com/Documentation/LeastSquaresFitting.pdf. Online; accessed at 5th November 2018.

Fischler, M. and Bolles, R. (1981). RANdom SAmpling Consensus: a paradigm for model fitting with application to image analysis and automated cartography. *Commun. Assoc. Comp. Mach.*, 24:358–367.

Grant, W. S., Voorhies, R., and Itti, L. (2013). Finding planes in lidar point clouds for real-time registration. In *International Conference on Intelligent Robots and Systems*, pages 4347–4354.

Hartley, R. and Zisserman, A. (2003). *Multiple view geometry in computer vision*. Cambridge University Press.

Nurunnabi, A. and andoderik Lindenbergh, Y. S. (2017). Robust cylinder fitting in three-dimensional point cloud dara. In *The International Archives of the Photogrammetry, Remote Sensing and Spatial Information Sciences*, pages 63–70.

Pereira, M., Silva, D., Santos, V. M. F., and Dias, P. (2016). Self calibration of multiple lidars and cameras on autonomous vehicles. *Robotics and Autonomous Systems*, 83:326–337.

Pratt, V. (1987). Direct Least-squares Fitting of Algebraic Surfaces. In *Proceedings of the 14th Annual Conference on Computer Graphics and Interactive Techniques*, SIGGRAPH '87, pages 145–152.

Tsai, A., Hsu, C., Hong, I.-C., and Liu, W.-K. (2010). Plane and boundary extraction from lidar data using clustering and convex hull projection. In *IAPRS*, pages 175–179.

APPENDIX

Plane Fitting. The implicit form of a 3D plane is usually given as $\begin{bmatrix} a & b & c & d \end{bmatrix} \begin{bmatrix} x & y & z & 1 \end{bmatrix}^T = 0$.

It can be written as $\mathbf{P}^T\mathbf{X} = \mathbf{X}^T\mathbf{P} = 0$ in short, where $\mathbf{P} = \begin{bmatrix} a & b & c & d \end{bmatrix}^T$ and $\mathbf{X} = \begin{bmatrix} x & y & z & 1 \end{bmatrix}^T$ contain the plane parameters and the point coordinates in homogeneous form. If the plane is represented by a point $\mathbf{P_0}$ and normal $\mathbf{n}$, then the implicit form is written as $\mathbf{n}^T\left(\hat{\mathbf{X}} - \mathbf{P}_0\right) = 0$, where $\hat{\mathbf{X}} = \begin{bmatrix} x & y & z \end{bmatrix}^T$. The two plane representations are equivalent if $\mathbf{P} = \begin{bmatrix} \mathbf{n}^T & -\mathbf{n}^T\mathbf{P}_0 \end{bmatrix}^T$ and $\mathbf{X} = \begin{bmatrix} \hat{\mathbf{X}} & 1 \end{bmatrix}$.

Plane fitting algorithms usually find the plane that is the closest one to the points. It can be carried out by minimizing the algebraic error: if a point set $\{P_i\}$, $i = \{1,2,\ldots,N\}$ is given, the cost function to be minimized becomes $\sum_{i=1}^{N}\left(\mathbf{X}_i^T\mathbf{P}\right)^2$.

This is equivalent to minimize the square of the norm of the matrix-vector product $\mathbf{AP}$: $\|\mathbf{AP}\|_2^2$, where $\mathbf{A} = \begin{bmatrix} \mathbf{X}_1^T & \mathbf{X}_2^T & \ldots & \mathbf{X}_N^T \end{bmatrix}^T$. It is well-known (Björck, 1996) that the optimal solution for this problem is that $\mathbf{P}$ is the eigenvector of matrix $\mathbf{A}^T\mathbf{A}$ corresponding to the smallest eigenvalue if the length of the vector, consisting of the plane parameters, is one: $\mathbf{P}^T\mathbf{P} = 1$.

Sphere Fitting. We have tried several sphere fitting algorithms on LiDAR point clouds, it was found that the method of (Eberly, c) is the most efficient one for this purpose, based on our experiences.

The equation of a general sphere is written as $(x-a)^2 + (y-b)^2 + (z-c)^2 = r^2$, where $\mathbf{C} = [a \quad b \quad c]^T$ is the center, and r the radius of the sphere.

The sphere fitting algorithm is based on minimizing squared error, where the error is defined as the difference between the estimated and real distance from a surface point to the center of the sphere: $E(a,b,c,r) = \sum_{i=1}^{N}(l_i - r)^2$,where $l_i = \sqrt{(x_i-a)^2 + (y_i-b)^2 + (z_i-c)^2}$ is the length of the radius to the i-th point (x_i, y_i, z_i).

The partial derivates of E with respect to r, a, b and c must be equal to zero at the minima. This leads to the following equations:

$$a = \frac{1}{N}\sum_{i=1}^{N} x_i + \frac{1}{N}\sum_{i=1}^{N} r\frac{a-x_i}{l_i}, \quad b = \frac{1}{N}\sum_{i=1}^{N} y_i + \frac{1}{N}\sum_{i=1}^{N} r\frac{b-y_i}{l_i},$$
$$c = \frac{1}{N}\sum_{i=1}^{N} z_i + \frac{1}{N}\sum_{i=1}^{N} r\frac{c-z_i}{l_i}, \quad r = \frac{1}{N}\sum_{i=1}^{N} l_i. \tag{2}$$

If one substitutes r into the last three equations, the center coordinates of the sphere can be estimated by fixpoint-iteration. The offset value is the average of the points. The four optimization steps are run one after the other until convergence.

Cylinder Fitting. We suggest to apply the method of (Eberly, a) for cylinder fitting.

A cylinder can be represented by a point $\mathbf{C}$ of the middle axis, and a direction, represented by unit vector $\mathbf{W}$, of the axis, and radius r. Furthermore, it can be defined two more unit vectors $\mathbf{U}$ and $\mathbf{V}$, which form in conjunction with $\mathbf{W}$ a right-handed orthonormal coordinate system. A surface point $\mathbf{X}$ of the cylinder can be written as $\mathbf{X} = \mathbf{C} + k\mathbf{U} + u\mathbf{V} + v\mathbf{W} = \mathbf{C} + R\mathbf{Y}$, where $R = \begin{bmatrix} \mathbf{U} & \mathbf{V} & \mathbf{W} \end{bmatrix}^T$ is a rotation matrix and $\mathbf{Y} = \begin{bmatrix} k & u & v \end{bmatrix}^T$ contains the coordinates of the point in the cylindric coordinate system.

When the distance between the axis and the surface point $\mathbf{X}_i$ is denoted by r_i, similar to the sphere, the error function becomes: $E(r^2, \mathbf{C}, \mathbf{W}) = \sum_{i=1}^{N}(r_i^2 - r^2)^2$,where $r_i^2 = u_i^2 + v_i^2$ is the distance of the point to the cylinder axis. The approximation of the radius is the average of the estimated radius lengths from the input surface points: $r = \frac{1}{N}\sum_{i=1}^{N} r_i$.

The axis point can be calculated by an iteration, where there is an offset value of the point, e.g. the mean of the input points, and every iteration replace the old value $\mathbf{C}$ for $\mathbf{C} + \alpha\mathbf{U} + \beta\mathbf{V}$. The α and β coefficients are obtained by the solution of the following expression:

$$\sum_{i=1}^{N}\begin{bmatrix} u_i^2 & u_iv_i \\ u_iv_i & v_i^2 \end{bmatrix}\begin{bmatrix} \alpha \\ \beta \end{bmatrix} = \frac{1}{2}\sum_{i=1}^{N}\begin{bmatrix} (u_i^2+v_i^2)u_i \\ (u_i^2+v_i^2)v_i \end{bmatrix}, \tag{3}$$

which is an inhomogeneous system of linear equations. Althought the solution seems to depend on $\mathbf{U}$ and $\mathbf{V}$, it can be justified that the axis point can be expressed with the $\mathbf{X}_i$ input points and only the $\mathbf{W}$ direction vector, because of $\mathbf{U}$, $\mathbf{V}$ and $\mathbf{W}$ form an orthonormal system by definition. Hence, the direction vector has to be approximated before the axis point.

The direction vector itself can be written by two parameters θ_0 and θ_1:

$$\mathbf{W} = (\cos\theta_0\sin\theta_1, \sin\theta_0\sin\theta_1, \cos\theta_1)$$
$$\theta_0 \in [0,2\pi) \qquad \theta_1 \in [0,\frac{\pi}{2}] \qquad w_z(\theta_0,\theta_1) \geq 0. \tag{4}$$

An exhaustive search finds the optimal parameters in our approach minimizing the cost function defined in Equation 4.